K-values-based upscaling of compositional simulation

Salehi, Amir; Voskov, Denis V.; Tchelepi, Hamdi A.

Important note
To cite this publication, please use the final published version (if applicable).
Please check the document version above.

K-Values-Based Upscaling of Compositional Simulation

Amir Salehi, Quantum Reservoir Impact and Stanford University;
Denis V. Voskov, Delft University of Technology; and **Hamdi A. Tchelepi,** Stanford University

Summary

Enhanced-oil-recovery (EOR) processes involve complex flow, transport, and thermodynamic interactions; as a result, compositional simulation is necessary for accurate representation of the physics. Flow simulation of compositional systems with high-resolution reservoir models is computationally intensive because of the large number of unknowns and the strong nonlinear interactions. Thus, there is a great need for upscaling methods of compositional processes. The complex multiscale interactions between the phase behavior and the heterogeneities lie at the core of the difficulty in constructing consistent upscaling procedures.

We use a mass-conservative formulation and introduce upscaled phase-molar-mobility functions for coarse-scale modeling of multiphase flow. These upscaled flow functions account for the subgrid effects caused by the absolute permeability and relative permeability variations, as well as the effects of compressibility. Upscaling of the phase behavior is performed as follows. We assume that instantaneous thermodynamic equilibrium is valid on the fine scale, and we derive coarse-scale equations in which the phase behavior may not necessarily be at equilibrium. The upscaled thermodynamic functions, which represent differences in the component fugacities, are used to account for the nonequilibrium effects on the coarse scale. We demonstrate that the upscaled phase-behavior functions transform the equilibrium phase space on the fine scale to a region of similar shape, but with tilted tie-lines on the coarse space. The numerical framework uses K-values that depend on the orientation of the tie-lines in the new nonequilibrium phase space and the sign of upscaled thermodynamic functions.

The proposed methodology is applied to challenging gas-injection problems with large numbers of components and highly heterogeneous permeability fields. The K-value-based coarse-scale operator produces results that are in good agreement with the fine-scale solutions for the quantities of interest, including the component overall compositions and saturation distributions.

Introduction

EOR processes usually involve complex flow, transport, and thermodynamic interactions in the subsurface formation. Numerical simulation is used to design and manage these complex EOR processes. Compositional flow simulation deals with coupled mass-conservation equations and thermodynamic equilibrium relations. These equations describe multicomponent transport in the presence of multiple flowing phases. Accurate description of how components partition across multiple fluid phases as they are transported in the porous medium is a major challenge. This is partly because the equations governing flow, transport, and thermodynamics are nonlinear and partly because of the tight coupling between the flow, transport, and mass transfer across the fluid phases. The challenge is made more severe by the fact that highly detailed representations of the reservoir and fluid models are necessary for field-scale simulation (Rannou et al. 2013). Flow simulation of compositional systems with high-resolution models is a computationally intensive effort because of the large number of unknowns and strong nonlinear effects. In the case of optimization or uncertainty quantification, large numbers of simulation runs are required (Shirangi and Durlofsky 2015; Volkov and Voskov 2016). The computational cost of such problems can be enormous. Therefore, accurate coarse-scale compositional simulation is of practical importance, and reliable techniques for upscaling of compositional displacements are necessary. The work flow of mapping and averaging the fine-scale reservoir and flow description to a coarse scale is referred to as upscaling.

Several researchers have investigated different aspects of the upscaling problem and proposed a wide variety of upscaling methods. One broad classification is dependent on whether the upscaled parameters are single-phase (e.g., upscaled absolute permeability, upscaled transmissibility), or two-phase (e.g., upscaled relative permeability, dispersion coefficient). Other aspects of upscaling are the boundary condition imposed (pressure, flux, effective flux), upscaling domains considered (local, extended local, global, and local/global), the types of grid used (nonuniform, flow-based, unstructured), and the nature of the displacement process (immiscible, miscible, compositional) (Hui 2005). Most of the techniques have focused on upscaling for single-phase flow or multiphase (transport) problems. There have also been a number of methods presented for upscaling of compositional simulation. Reviews and comparative studies (Christie 1996; Barker and Thibeau 1997; Farmer 2002; Durlofsky and Chen 2012) provide detailed discussions on various methods and outstanding issues. Single-phase-flow upscaling (Durlofsky 1991; Chen et al. 2003; Wu et al. 2008; Zhang et al. 2008) attempts to capture the fine-scale features of the flow by calculating an equivalent permeability ($\mathbf{k}^*$) or transmissibility (T^*) that predicts the same total single-phase flow through a homogeneous coarse block as the summation of flow through all underlying fine blocks. Single-phase upscaling represents the most commonly applied upscaling technique in practice. It is also a prerequisite for more-general (multiphase or compositional) problems.

Although single-phase-upscaling techniques can provide satisfactory results for problems of two- and three-phase flow in some cases, they only consider the single-phase-pressure equation. Hence, parameters involved in the transport equations (i.e., relative permeability and capillary pressure) are not considered. Upscaling errors become more pronounced in the case of high-mobility-ratio displacements and large upscaling ratios where numerical diffusion can affect the transport significantly. To treat this, multiphase-upscaling techniques are needed, and they target multiphase properties, such as relative permeability relations and fractional-flow functions. The Kyte and Berry (1975) and Stone (1991) methods are the two widely used techniques. Many of the subsequent methods can be seen as extensions. Various techniques (local, global, and local/global) were developed and tested by Barker and Thibeau (1997), Barker and Dupouy (1999), Darman et al. (2002), Chen and Durlofsky (2006), and Wallstrom et al. (2002).

Previous studies of upscaling compositional flow simulation fall into three categories. The first type is to introduce one more continuum to represent the bypassed fraction of the reservoir volume. Fayers et al. (1989) proposed a dual-zone-mixing procedure for representing the averaging effect of the fine-scale heterogeneities in an equation-of-state (EOS) compositional model. Separate phase-behavior calculations are performed for contacted and bypassed zones to model the nonuniform phase behavior. The mass flux between zones can represent the nonequilibrium behavior at the subgrid scale. Evazi and Jessen (2014) and Zhang and Okuno (2015) developed a similar approach to dual-zone mixing. The pore space is arranged into two levels of porosity depending on flow contribution, and a dual-porosity/dual-permeability flow model is adapted for coarse-scale flow simulation. However, the dual-porosity model may be too time-consuming to be used for field-scale applications (Coats et al. 2004). Apart from computational efficiency, a single-porosity model may be preferred in terms of the computational robustness. In Peng et al. (2009), for example, the dual-porosity model showed convergence issues in simulating strongly heterogeneous reservoirs.

A second type of method involves the use of so-called transport coefficients (α-factors) computed for each component in each phase to capture the averaged fine-scale fluxes of each component (Barker and Fayers 1994). The α-factors were used to capture the partitioning of components into the oil and gas phases in coarse-scale models. These coefficients are then used in conjunction with pseudo-relative permeabilities to perform compositional flow simulations. Christie and Clifford (1998) used an extended local region along with streamline techniques to generate the fine-scale solution needed to calculate α-factors. However, in their work, no upscaled relative permeability functions were used because they only considered problems of single-phase flow. Ballin et al. (2002) applied the transport-coefficients method for a field case with a rich gas/condensate fluid. Ogunlana and Mohanty (2005) investigated the use of α-factors for 2D and 3D fractured models. However, their model was not a multiphase-flow problem, and only a gas phase was present. Li and Durlofsky (2016) (see also Li 2014) have extended the method of transport coefficients to include treatment for near-well upscaling. They also developed transport-coefficient-based frameworks for ensemble-level and local/global compositional upscaling procedures.

The third type of method is to adjust thermodynamic properties of the components to match fine-scale fluxes in a coarse-scale simulation. A fundamental assumption for compositional simulation is the local equilibrium assumption, where fluids are perfectly mixed and in equilibrium within individual gridblocks. This assumption may be valid at small length scales, where diffusive effects ensure good mixing, but subgrid heterogeneities cause variations in fluid compositions to scales smaller than the size of typical gridblocks. Iranshahr et al. (2014) and Indrupskiy et al. (2016) proposed a novel compositional upscaling methodology derived from a nonequilibrium thermodynamic formulation. They developed a mass-conservative formulation and introduced an upscaled molar mobility for each phase. The framework assumes instantaneous thermodynamic equilibrium on the fine scale and introduces nonequilibrium functions to correct phase behavior on the coarse scale. The deviation from local equilibrium is quantified by coarse-scale thermodynamic functions (Zubov et al. 2016). Conversion of the nonequilibrium thermodynamic functions into the thermodynamically consistent transport coefficients was described by Salehi et al. (2012, 2013). We note that in related work presented in a companion paper, Salehi et al. (2016) extended the formulation and provided comparisons with standard techniques of compositional upscaling (transport coefficients) for various challenging gas-injection problems.

Flash calculations can be responsible for a significant fraction of computational time in compositional reservoir-simulation models. The most widely used approach to represent the phase equilibrium is an iterative process dependent on an EOS (Coats 1980; Aziz and Wong 1988). It is possible to simplify the EOS computations by assuming that components partition across phases with a fixed ratio (K-value), and these K-values depend on pressure and temperature, but are weak functions of composition (Bolling 1987). If the pressure is low enough for many gas/oil systems, a critical point will not be present, and K-values will depend only weakly on composition (Orr 2007). In many practical oil-recovery problems, the K-values are indeed weak functions of composition, and this makes the constant-K-value model an efficient approximation. In this work, the global compositional upscaling procedure is incorporated into a K-values-based compositional simulation formulation. We use the upscaled nonequilibrium thermodynamic functions to transform the equilibrium phase space from the fine scale to a modified region of similar shape, but with tilted tie-lines on the coarse scale. Using the orientation of tie-lines in the new nonequilibrium phase space and the sign of upscaled thermodynamic functions, we develop a framework to compute a modified set of K-values. These new K-values can then be directly used for the coarse-scale simulation to account for nonequilibrium effects on the coarse scale.

This paper proceeds as follows. First, the K-values-based fine- and coarse-scale compositional formulations are presented. We then present the detailed methodology for computing all upscaled parameters and functions. The proposed methodology is then applied to various challenging gas-injection problems with a large number of components and highly heterogeneous permeability fields. The model problems considered here neglect the effects of capillarity and gravity. This type of flow is usually encountered in field-scale flow simulation of petroleum reservoirs. The capillarity effects are often ignored for flow at such large scales. For the cases such as gravity drainage where gravity is important, the upscaling method proposed in this work may be extended to account for the effects of gravity. In the problems with gravity segregation, compositions may change because of flow in the z-direction. This leads to changes in thermodynamics, and therefore the extension to include gravity effects requires further analysis. We demonstrate that the modified set of K-values efficiently improves the accuracy of coarse-scale results to reproduce averaged fine-scale solutions such as component overall compositions and phase saturation. Finally, we conclude by summarizing the main findings and present our recommendation for future work.

K-Values-Based Fine-Scale Compositional Formulation

We consider an isothermal system in which the total number of components is N_c and the total number of phases is N_p. Capillary pressure, diffusive effects, chemical reactions, and rock adsorption are neglected. The full system of conservation equations that describes flow and transport of multiphase multicomponent fluid on fine scale can be written as

$$\frac{\partial}{\partial t}\left(\phi^f \sum_{j=1}^{N_p} x_{ij}^f \rho_j^f S_j^f\right) - \nabla\left(\sum_{j=1}^{N_p} x_{ij}^f \rho_j^f \lambda_j^f \mathbf{k}^f \cdot \nabla p^f\right) + \sum_{j=1}^{N_p} x_{ij}^f \rho_j^f q_j^f = 0, \quad i = 1,...,N_c, \quad \dots\dots\dots\dots\dots\dots\dots\dots\dots \quad (1)$$

where superscript f indicates a fine-scale quantity; ϕ is porosity; t is time; x_{ij} is the mole fraction of component i in phase j; ρ_j is the molar density of phase j; S_j is the saturation (volume fraction) of phase j; u_j is the Darcy-flow velocity of phase j; $\mathbf{k}$ is absolute permeability; $\lambda_j^f = k_{rj}^f/\mu_j^f$ is the phase mobility, with k_{rj}^f and μ_j^f being the relative permeability and viscosity of phase j; p is pressure, which is assumed to be the same for all the phases in the absence of capillary effects; and q_j is the source/sink term for phase j. Both λ_j^f and k_{rj}^f are functions of phase saturation. For a complete list of symbols, refer to the Nomenclature section. Local constraint equations for instantaneous thermodynamic phase equilibrium using an EOS-based compositional model are

$$f_{i1}(p,T,x_1) = f_{ij}(p,T,x_j), \quad i=1,\ldots,N_c; \; j=2,\ldots,N_p \quad\ldots\ldots\ldots\ldots\ldots\ldots\ldots\ldots\ldots\ldots\ldots\ldots\ldots\ldots\ldots\ldots \quad (2)$$

$$\sum_{i=1}^{N_c} x_{ij} = 1, \quad j=1,\ldots,N_p \quad\ldots\ldots\ldots\ldots\ldots\ldots\ldots\ldots\ldots\ldots\ldots\ldots\ldots\ldots\ldots\ldots\ldots\ldots\ldots\ldots\ldots\ldots \quad (3)$$

$$\sum_{j=1}^{N_p} S_j = 1, \quad\ldots\ldots\ldots\ldots\ldots\ldots\ldots\ldots\ldots\ldots\ldots\ldots\ldots\ldots\ldots\ldots\ldots\ldots\ldots\ldots\ldots\ldots\ldots\ldots\ldots\ldots\ldots\ldots \quad (4)$$

where f_{ij} is the fugacity for component i in phase j. The value of f_{ij} is a function of pressure, temperature, and phase compositions and is usually computed from an EOS. Eq. 2 states that fine-scale gridblocks are assumed to be complete mixing cells at chemical equilibrium and the component partial fugacities are equal among all the phases. The system of equations presented consists of a coupled set of $N_p(N_c+1)+1$ equations and local constraints. After deriving the discrete finite-volume formulation, the governing equations and constraints are solved for unknown variables (one pressure, N_p phase saturations, and $N_c \times N_p$ phase compositions) for each gridblock. Defining equations and unknowns here are derived from the natural-variables formulation (Coats 1980; Cao 2002).

Phase-Behavior Calculation. Compositional simulations describe multicomponent transport in the presence of multiple flowing phases. Accurate description of how components partition across multiple fluid phases as they are transported in the porous medium is a major challenge. This will add complexity to the compositional modeling compared with the black-oil models. Thermodynamic phase behavior needs to be modeled for each gridblock and at every Newton iteration. For the natural-variables formulation, the thermodynamic phase-behavior calculation includes two steps: phase-stability test (Michelsen 1982a) for gridblocks that have single-phase status, and phase-split (flash) calculations (Michelsen 1982b) for gridblocks that changed their phase state from single phase to two phase. The thermodynamic statuses of all gridblocks are checked at the end of each Newton iteration while solving the coupled nonlinear system. For gridblocks in single-phase (gas or oil) status, if the phase-stability test indicates that the single-phase status is not stable (status changes to two phase), then flash calculations are performed to calculate the amount and compositions of the two phases formed in the gridblock as the initial guess for the next nonlinear iteration. This requires modification in the set of equations and unknowns to account for the appearance of the new phase. Thermodynamic phase-behavior (flash) calculations can be either dependent on equilibrium ratios (K-values) or an iterative process derived from an EOS. The ultimate objective is to determine the phase fraction, phase compositions, and phase density at a given pressure, temperature, and overall compositions. Note that in the application of compositional simulation for practical field problems, the phase-stability test can be a very expensive computational kernel (for natural-variables formulation). Therefore, robust and efficient techniques have been developed to reduce, or eliminate, the computational cost of this step (Rasmussen et al. 2003; Voskov and Tchelepi 2009a, b; Pan and Tchelepi 2011; Iranshahr et al. 2013a, b).

Compositional Space. In this subsection, we briefly describe the representation of thermodynamic phase behavior in compositional space. A typical gas/oil-phase diagram for a three-component system is shown in **Fig. 1,** which displays phase-behavior information at a fixed pressure and temperature. The dimension of the compositional space depends on the number of components, N_c. A multicomponent mixture can be represented as a point in this space and the overall composition of a component, z_i, is given by the perpendicular distances from the composition point to the appropriate side of the compositional space. The corners of the diagram represent 100% of the component with which the corner is labeled.
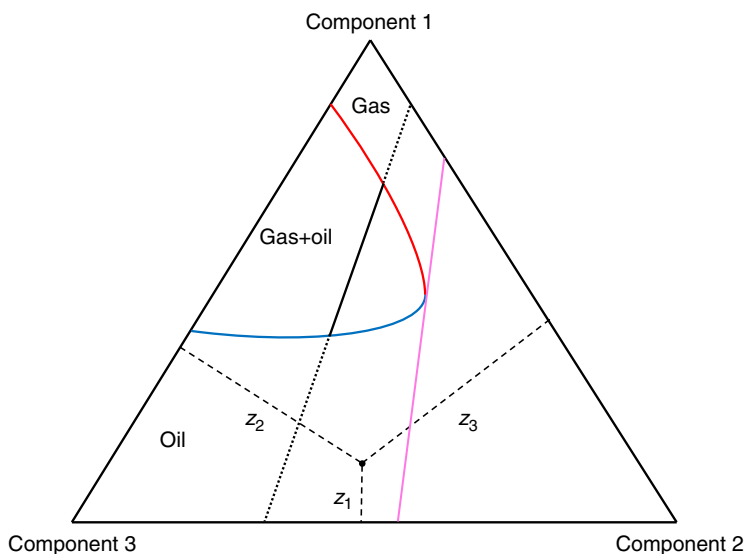
Fig. 1—Ternary diagram showing compositional space for three-component mixtures. A tie-line connects the bubblepoint mixture (represented by the blue curve) to the corresponding dewpoint mixture (represented by the red curve).

The sides of the ternary diagram represent binary mixtures of the two components that lie on that side. For gas/oil systems, the component at the top corner of the diagram is usually the lightest component, and the heaviest component is usually placed at the bottom-left corner. Any mixture of two overall compositions, whether either is single phase, must lie on a straight line that connects those compositions (Orr 2007). In the compositional space, the gas/oil mixtures that are at thermodynamic equilibrium are connected by a tie line and the overall composition of any mixture along the tie line can be expressed as a linear combination of the tie-line endpoints:

$$z_i = \nu_g x_{ig} + (1 - \nu_g)x_{io} \equiv \nu y_i + (1 - \nu)x_i, \quad i = 1, ..., N_c, \quad \text{...........................} \quad (5)$$

where in the two-phase system considered here, $\nu_g \equiv \nu$ is the molar fraction of gas phase, $\nu_o \equiv 1 - \nu$ is the molar fraction of oil phase, and x_{ig} and x_{io} represent the compositions of component i in gas and oil phases that are replaced by y_i and x_i (equilibrium tie-line endpoints), respectively. The value of ν changes between zero and unity inside the two-phase region. The region of overall compositions in Fig. 1 that form two phases is enclosed by the loci of liquid- and vapor-phase compositions, which is known as the binodal curve. A set of tie-lines connects all the bubblepoint mixtures (blue curve in Fig. 1, $\nu = 0$) to the corresponding dewpoint mixtures (red curve in Fig. 1, $\nu = 1$). With changes in pressure, temperature, or compositions, the length of the tie-line approaches zero, yielding the critical tie-line. Tie-lines do not exist beyond the critical condition.

K-Values Model. The general EOS-based compositional model has wide applicability. However, it has several disadvantages. First, rigorous phase-stability analysis and flash calculations are iterative processes that can consume significant computational time. Another problem is that the fugacity relations are highly nonlinear, and this makes it difficult to analyze the complex coupling of the thermodynamics with multiphase flow and multicomponent transport. The K-values model can improve the efficiency of the phase-behavior computation. In addition, it provides a simpler form of the mathematical statement that facilitates detailed nonlinear analysis. However, note that K-values-based compositional simulation has certain limitations to model miscible or near-miscible gas-injection processes. For upscaling these more-complicated compositional processes, the nonequilibrium-based full EOS upscaling techniques described in Salehi et al. (2013) may be used. Here, we describe the main principles of the K-values approach for two-phase systems. At equilibrium, a two-phase mixture will satisfy

$$K_i = \frac{y_i}{x_i} = \frac{\hat{\phi}_{io}}{\hat{\phi}_{ig}}, \quad i = 1, ..., N_c, \quad \text{.....................................} \quad (6)$$

where y_i and x_i are the mole fractions of component i in the vapor and liquid phases, respectively, and K_i is the equilibrium ratio (also known as the K-value). $\hat{\phi}_{ij}$ is the partial-fugacity coefficient of component i in phase j, defined by

$$\hat{\phi}_{ij} = \frac{f_{ij}}{x_{ij}p}, \quad i = 1, ..., N_c. \quad \text{.......................................} \quad (7)$$

The Wilson equation is frequently used to estimate equilibrium K-values:

$$K_i = \frac{P_{ci}}{P} \exp\left[5.37(1 + \omega_i)\left(1 - \frac{T_{ci}}{T}\right)\right], \quad \text{.............................} \quad (8)$$

from which phase molar fractions and compositions can be estimated by the Ratchford-Rice equation:

$$F(\nu) = \sum_{i=1}^{N_c} \frac{z_i(1 - K_i)}{\nu(K_i - 1) + 1} = 0. \quad \text{..................................} \quad (9)$$

In general, K-values depend on pressure, temperature, and overall composition. Rannou et al. (2013) proposed a tie-line-based approach to account for K-value dependencies on compositions in addition to pressure and temperature in compositional simulation. In this work, we shall assume that K-values are constant. This is often a good approximation for many hydrocarbon systems at moderate pressures and temperatures (Orr 2007). When this is not the case, the methodology presented here must be understood as the building block for an overall flash calculation in which an outer iteration is performed to determine the K-values on the fine scale (Juanes 2008). One of the limitations of K-values is their application for near-miscible compositional displacements. The fugacity constraint described by Eq. 2 can now be rewritten as

$$f_{io} - f_{ig} = 0 \Rightarrow K_i^f x_i - y_i = 0, \quad i = 1, ..., N_c. \quad \text{............................} \quad (10)$$

For fine-scale formulation, we perform the flash calculation with the constraint of equal component fugacity among phases. If K-values are constant, then the liquid and vapor portions of the binodal curve are straight lines on a ternary diagram. For a ternary system with constant K-values, the two-phase region must be a band across the diagram that intersects the two sides with one K-value greater than unity and the other K-value less than unity. As an illustrative example to explain the discussed materials, we consider a three-component system: methane/carbon dioxide (CO_2)/C_{10}. **Fig. 2** shows a phase diagram for $K_1 = 2.6$, $K_2 = 1.5$, and $K_3 = 0.01$. These K-values represent the phase behavior of this ternary system at $p = 110$ bar and $T = 450$ K. The compositions of injected gas and initial oil are described in **Table 1**. For example, on the CO_2/C_{10} side of the diagram, we have

$$x_2 = \frac{1 - K_3}{K_2 - K_3}, \quad y_2 = K_2 \frac{1 - K_3}{K_2 - K_3}. \quad \text{...............................} \quad (11)$$

K-Values-Based Coarse-Scale Compositional Formulation

An accurate simulation of compositional processes on a coarse grid implies upscaling of the coupled system of flow, transport, and thermodynamic equations. We presented a detailed procedure for derivation and calculation of upscaled single- and multiphase-flow parameters in a companion paper (Salehi et al. 2016). However, a brief description of flow-upscaling procedure is presented here (Eqs. 15 through 19). Upscaled-flow functions account for the subscale relative permeability variation as well as compressibility effects. These functions make it possible for a coarse-grid model to move the correct amounts of phases and components across coarse interfaces. However, it is also necessary to split those components into the correct gas and liquid fractions to reproduce fine-scale solutions.

Upscaling of nonlinear flash equation is a problem that is specific to compositional modeling, and is the main focus of this work. If we solve Eq. 9 n times for a set of n fine gridblocks or if we solve it only one time by regrouping those n cells into a coarse gridblock, the phase description that will be obtained in each instance may be very different. In other words, flash equations cannot be averaged out over several gridblocks and fine-scale K-values are not sufficient to describe the phase behavior on coarser scales. The averaging

problem occurs when the *K*-values correlation is strongly dependent on pressure or composition, or if all the underlying fine cells in a coarse gridblock are not in the same region of the phase diagram. Here, we introduce a *K*-values-based coarse-scale operator for compositional simulation. The correction in phase splitting is performed by modifying *K*-values on the coarse scale. We take the form of coarse-scale mass-conservation equations as

$$\frac{\partial}{\partial t}\left(\phi^* \sum_{j=1}^{N_p} x_{ij}^c \rho_j^c S_j^c\right) - \nabla\left(\sum_{j=1}^{N_p} x_{ij}^c \rho_j^* \lambda_j^* \mathbf{k}^* \cdot \nabla p^c\right) + \sum_{j=1}^{N_p} x_{ij}^c \rho_j^c q_j^c = 0, \quad i = 1, ..., N_c. \quad \dots \dots \dots \dots \dots \dots \dots (12)$$
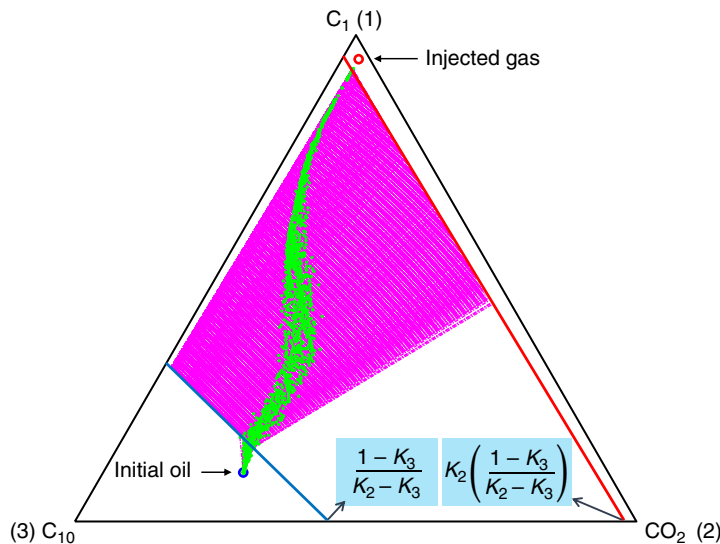
Fig. 2—Ternary phase diagram for a system with constant *K*-values = $K_1 = 2.6$, $K_2 = 1.5$, and $K_3 = 0.01$. A set of tie-lines connects the bubblepoint mixtures (represented by the blue curve) to the corresponding dewpoint mixtures (represented by the red curve). The fine-scale compositional path from injected gas to the initial oil in place is shown by green dots.

	C_1	CO_2	C_{10}
Initial oil	0.10	0.25	0.65
Injected gas	0.95	0.02	0.03

Table 1—Compositions of initial oil and injected gas for Fig. 2.

To provide fine-scale compositional features on the coarse scale, we apply a modified version of the fugacity constraint on the coarse-scale system:

$$f_{ig}(y_i^c, \overline{p}, T) - f_{io}(x_i^c, \overline{p}, T) = \Delta f_i^*, \quad i = 1, ..., N_c. \quad \dots \dots \dots \dots \dots \dots \dots \dots \dots \dots \dots \dots \dots \dots (13)$$

Using *K*-values in the fugacity constraint, the nonequilibrium source term will be computed as

$$\Delta f_i^* = f_{ig}(y_i^*, \overline{p}, T) - f_{io}(x_i^*, \overline{p}, T) \equiv y_i^* - K_i^f x_i^*, \quad i = 1, ..., N_c, \quad \dots \dots \dots \dots \dots \dots \dots \dots \dots \dots (14)$$

where y_i^* and x_i^* are the compositions of lumped gas phase and oil phase on the coarse scale, respectively (Eq. 22). Depending on the sign of Δf_i^*, *K*-values will be modified for the coarse-scale simulation. If Δf_i^* is positive, it indicates that fugacity of component *i* is higher in the gas phase compared with the oil phase, and we need a higher *K*-value on the coarse scale to compensate for this nonequilibrium effect (positive Δf_i^*). On the other hand, if Δf_i^* is negative, a lower *K*-value should be used to decrease the fugacity of component *i* in the oil phase and make it less volatile on the coarse scale. For heavier components (e.g., C_{10} in this case), the absolute value of Δf_i^* is negligible. Therefore, a "non-sensible" change in *K*-value for coarse-scale simulation is needed. For the constant *K*-values system presented in Fig. 2, we perform the phase-behavior upscaling using nonequilibrium functions. The fine model (100×20) is scaled up to a 100×1 model. The averaged fine- and coarse-scale compositional paths are shown in **Fig. 3**. The coarse-scale solution path follows a new set of tie-lines (shown in blue), which is tilted with respect to the fine-scale tie-lines. The slope of this new set of tie-lines represents the *K*-values on the coarse scale.

The overall algorithm for the coarse-scale modeling of compositional flow problems is summarized as the following six steps.

Step 1. Solve the global fine-scale compositional flow problem with generic boundary conditions (i.e., flow in the *x*- and *y*-direction, respectively, for a 2D problem) to obtain fine-scale flow solutions—pressure (*p*), phase saturation (S_j), molar-phase density (ρ_j), and phase-molar compositions—for each component (x_{ij}). The upscaled single-phase-flow parameters ($\mathbf{k}^*$ or T^*) can be computed using any single-phase-upscaling (SPU) method, from global fine-scale single-phase solutions, or any other local or local/global approaches. We compute T_x^* such that the integrated fine-scale flow rate through the coarse interface is the same as the coarse-scale solution:

$$T_x^* = \frac{\sum_l (q^f)_l}{(p_m^c - p_{m+1}^c)}, \quad \dots \dots \dots \dots \dots \dots \dots \dots \dots \dots \dots \dots \dots \dots \dots \dots \dots \dots \dots \dots \dots \dots (15)$$

where $p_m^c = \langle p^f \rangle_m$ is the pore-volume average pressure values of underlying fine gridblocks in coarse gridblock m. Similarly, T_y^* and T_z^* are computed for y- and z-direction.
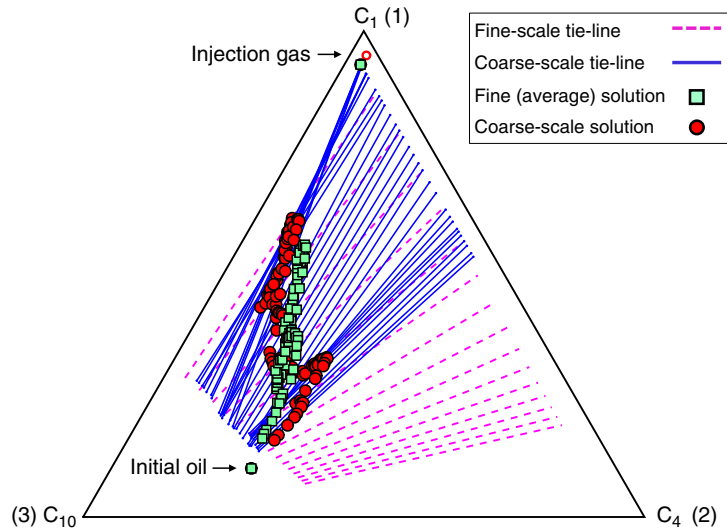
Fig. 3—Ternary diagram for a system with constant *K*-values. Fine-scale tie-lines are shown in pink and coarse-scale tie-lines are shown in blue. Slopes of the tie-line set represent *K*-values. The averaged fine-scale compositional path from injected gas to the initial oil is shown by green dots. Red dots demonstrate the coarse-scale compositional path.

Step 2. From the global fine-scale solution, compute upscaled phase-molar mobility $(\rho_j \lambda_j)^*$ as a function of upstream coarse-gridblock gas saturation (S_g^*). The upscaled phase-molar-mobility functions are computed such that the integrated fine-scale flux of each phase is captured in the coarse-scale model. For every direction (x, y, or z), a separate table of these dynamic functions (per coarse interface) should be generated. Note that if the boundary conditions and/or fluid properties are changed significantly, then the corresponding fine-scale solution may be needed to generate upscaled functions.

$$\overline{\rho_g q_g} = \sum_{l_g} (\rho_g^f \lambda_g^f T^f \Delta p^f)_{l_g} + \sum_{l_{go}} (\rho_g^f \lambda_g^f T^f \Delta p^f)_{l_{go}}, \quad \dots \dots \dots \dots \dots \dots \dots \dots \dots \dots \dots \dots \dots \dots \dots \dots (16)$$

$$\overline{\rho_o q_o} = \sum_{l_o} (\rho_o^f \lambda_o^f T^f \Delta p^f)_{l_o} + \sum_{l_{go}} (\rho_o^f \lambda_o^f T^f \Delta p^f)_{l_{go}}, \quad \dots \dots \dots \dots \dots \dots \dots \dots \dots \dots \dots \dots \dots \dots \dots \dots (17)$$

$$(\rho_j \lambda_j)^* = \frac{\overline{\rho_j q_j}}{T^*(p_m^c - p_{m+1}^c)}, \quad \dots \dots \dots \dots \dots \dots \dots \dots \dots \dots \dots \dots \dots \dots \dots \dots \dots \dots \dots \dots \dots (18)$$

$$S_g^* = \overline{S_g} = \frac{\sum_l \phi^f V^f S_g^f}{\sum_l \phi^f V^f}, \quad \dots \dots \dots \dots \dots \dots \dots \dots \dots \dots \dots \dots \dots \dots \dots \dots \dots \dots \dots \dots \dots \dots (19)$$

where l_g, l_o, and l_{go} are the indices of fine gridblocks or interfaces in single-phase gas, single-phase oil, and two-phase regions, respectively.

Step 3. The upscaled thermodynamic functions are also computed for all the coarse-scale gridblocks (as opposed to coarse-scale interfaces) using the global fine-scale solution (Salehi 2016).

For a given coarse gridblock, compute the molar amount of component i (n_{ig}^* and n_{io}^*), and the total molar amount of each phase ($n_{\text{tot},g}^*$ and $n_{\text{tot},o}^*$):

$$n_{\text{tot},g}^* = \sum_{i=1}^{N_c} n_{ig}^* = \sum_{l_g} \phi^f V^f \rho_g^f + \sum_{l_{go}} \phi^f V^f S_g^f \rho_g^f, \quad i = 1, \dots, N_c, \quad \dots \dots \dots \dots \dots \dots \dots \dots \dots \dots \dots (20)$$

$$n_{\text{tot},o}^* = \sum_{i=1}^{N_c} n_{io}^* = \sum_{l_o} \phi^f V^f \rho_o^f + \sum_{l_{go}} \phi^f V^f S_o^f \rho_o^f, \quad i = 1, \dots, N_c. \quad \dots \dots \dots \dots \dots \dots \dots \dots \dots \dots \dots (21)$$

With the molar amounts computed previously, calculate the averaged lumped-phase compositions on the coarse scale (y_i^* and x_i^*):

$$y_i^* = \frac{n_{ig}^*}{n_{\text{tot},g}^*}, \quad x_i^* = \frac{n_{io}^*}{n_{\text{tot},o}^*}. \quad \dots \dots \dots \dots \dots \dots \dots \dots \dots \dots \dots \dots \dots \dots \dots \dots \dots \dots \dots \dots (22)$$

Compute the upscaled phase densities (ρ_g^* and ρ_o^*).

Compute the upscaled fugacity functions (Δf_i^*) using the average phase compositions computed previously, as a function of coarse-gridblock saturation (Eq. 14). These upscaled fugacity functions will be included in the fugacity constraint and will be solved together with the flow and transport equations to account for nonequilibrium effects on the coarse scale (Eq. 13).

Step 4. With all the upscaled parameters/functions obtained (upscaled single-phase-flow parameters, upscaled phase-molar-mobility functions, upscaled phase densities, and upscaled thermodynamic fugacity functions), perform the coarse-scale compositional flow simulation.

Step 5. Compute the modified K-values for coarse-scale simulation using the results of nonequilibrium simulation. The slopes of tielines on the coarse scale (blue lines in Fig. 3) correspond to the modified K-values for the coarse model. We compute

$$K_i^c = \frac{y_i^{c,NE}}{x_i^{c,NE}}, \quad i = 1, ..., N_c. \quad\dots\dots\dots\dots\dots\dots\dots\dots\dots\dots\dots\dots\dots\dots\dots\dots\dots \quad (23)$$

Step 6. With upscaled flow functions and a modified set of K-values, perform the coarse-scale compositional flow simulation.

Finally, we compare the coarse-scale solutions to the (averaged) fine-scale solutions to assess the quality of the results and check if the coarse model can sufficiently reproduce important fine-scale flow behavior.

Numerical Results

Here, we apply the compositional upscaling procedure to two numerical examples. We consider cases with different numbers of components, thermodynamics complexity, and strong heterogeneity conditions. We use channelized permeability fields with large coarsening ratios to test the robustness of our upscaling framework. Coarse-scale results are compared with fine-scale reference solutions to assess the accuracy of different upscaling techniques. We have implemented the K-values-based nonequilibrium compositional upscaling framework in the Automatic Differentiation General Purpose Research Simulator (Zhou et al. 2011; Voskov 2012; Voskov and Tchelepi 2012; Zhou 2012; Iranshahr et al. 2013a, b). The fine-scale relative permeability functions are quadratic functions of saturation values with Corey oil and gas exponent of 2: $k_{rg}^f = (S_g^f)^2$ and $k_{ro}^f = (1 - S_g^f)^2$.

Case 1: Horizontal Layer of SPE10. This case involves a heterogeneous 2D $(x - y)$ model taken from the 80th layer of the SPE10 problem (Christie and Blunt 2001). The 2D fine-scale model (220×60) is scaled up to 55×15 (upscaling ratio: 16) and also to 22×6 (upscaling ratio: 100), as shown in **Fig. 4**. We consider different large upscaling ratios to test the robustness of upscaling methodologies. Porosity is specified as $\phi = 0.20$ and is constant for all the gridblocks. The fine-scale cells are of size $\Delta x = 3$ m, $\Delta y = 6$ m, and $\Delta z = 0.6$ m. Initially, the reservoir contains only the oil phase, which is a mixture of four components: C_1 (10%), CO_2 (18.09%), C_4 (37.66%), and C_{10} (34.25%). We inject a four-component gas—C_1 (97%), CO_2 (1%), C_4 (1%), and C_{10} (1%)—through the left boundary at 100 bar and produce through the right boundary at 70 bar. This set of components was considered in Orr (2007) and corresponds to an immiscible system (**Table 2**). Initial reservoir pressure is 85 bar. The displacement is isothermal at 373 K, and we run the simulation for 400 days.
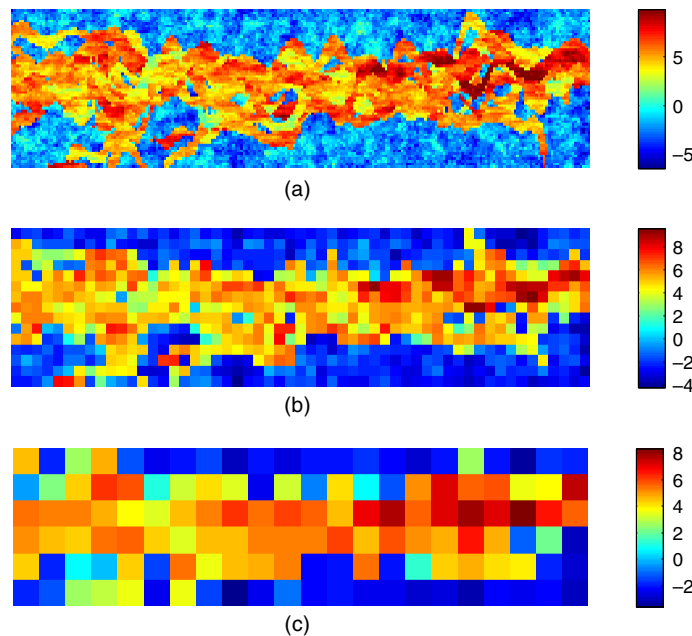

Fig. 4—Permeability fields (log k) for (a) fine scale (220×60), (b) coarse scale (55×15), (c) coarse scale (22×6), Case 1.

|	C_1	CO_2	NC_4	C_{10}
Initial oil	0.10	0.1809	0.3766	0.3425
Injected gas	0.97	0.01	0.01	0.01

Table 2—Compositions of initial oil and injected gas, Case 1.

Using the global fine-scale solution, the Δf_i^* functions are computed for all the coarse gridblocks. **Fig. 5** shows the Δf_i^* distributions of all four components for two different coarsening ratios. The nonequilibrium functions have the largest values for the lightest component and decrease as the component molecular weight increases (e.g., C_{10}). In other words, the lightest components experience the largest nonequilibrium effects on the coarse scale, and, as a result, need more modification in terms of K-value. The key assumption for the fine-scale gridblocks is that of complete vapor/liquid equilibrium, and as expected, the Δf_i^* functions show larger values (for all the components) as the coarsening ratio increases from 16 to 100.
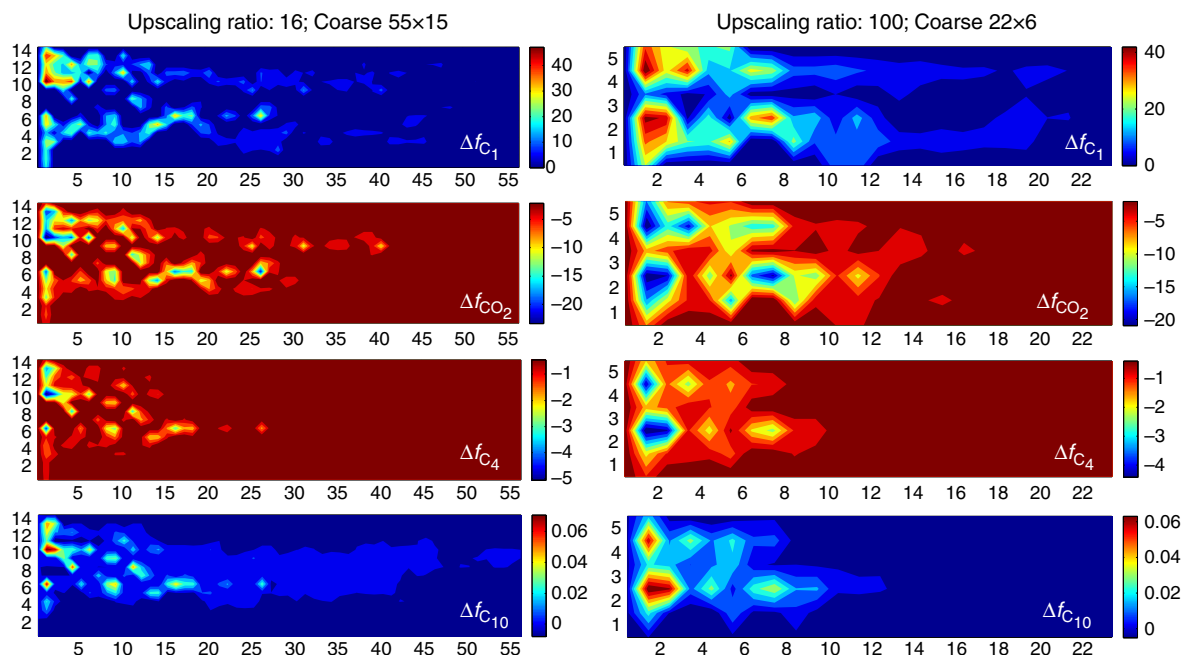
Fig. 5—(Left) Nonequilibrium functions for all four components (upscaling ratio: 16); **(right)** nonequilibrium functions for all four components (upscaling ratio: 100), Case 1.

For the lightest component (C_1), Δf_1^* is always positive throughout the entire simulation. This indicates that fugacity of C_1 is higher in the gas phase compared with the oil phase, and a higher K-value for this component is needed to account for the positive nonequilibrium effect. CO_2 and C_4 demonstrate opposite behaviors on the coarse scale with negative nonequilibrium function, which leads to a smaller K-value on the coarse scale for these components. Δf_4^* for the heaviest component in this case (C_{10}) is very close to zero. Therefore, the required modification of the K-value on the coarse scale is negligible. The modified K-values for the coarse-scale model are computed and demonstrated for all four components in **Fig. 6** (coarsening ratio of 16). **Fig. 7** demonstrates the modified K-values for coarsening ratio of 100. An average K-value for each component is computed for the coarse-scale simulation and is summarized in **Table 3**. As the coarsening ratio increases from 16 to 100, the corresponding K-values also change consistently (either increase or decrease).
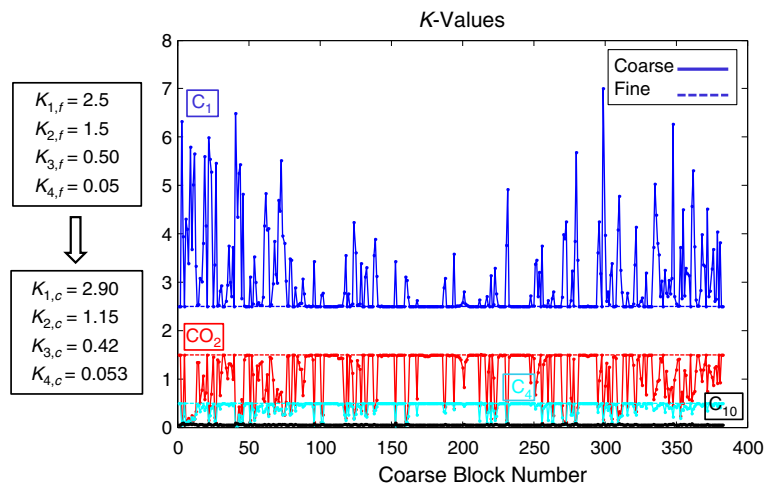
Fig. 6—Set of *K*-values for fine- and coarse-scale (55×15) simulations, Case 1.

Fig. 8 shows the C_1 concentration distributions at 230 days for fine, averaged fine, and modified K-value technique. Next, we compute errors for upscaled models relative to averaged fine-scale results for gas saturation and overall compositions maps. These errors, denoted E_s and E_{z_i}, are computed as

$$E_s^c = \left[\frac{1}{N_b} \sum_{m=1}^{N_b} \left(S_{g,m}^c - \langle S_g^f \rangle_m \right)^2 \right]^{1/2}, \quad \dots \dots \dots \dots \dots \dots \dots \dots \dots \dots \dots \dots \dots \dots \dots \quad (24)$$

$$E_{z_i}^c = \frac{\left[\frac{1}{N_b} \sum_{m=1}^{N_b} \left(z_{i,m}^c - \langle z_i^f \rangle_m \right)^2 \right]^{1/2}}{\left| z_i^{\text{inj}} - z_i^{\text{prod}} \right|}, \quad \dots \dots \dots \dots \dots \dots \dots \dots \dots \dots \dots \dots \quad (25)$$

where N_b is the total number of coarse gridblocks, $\langle S_g^f \rangle_m$ denotes the pore-volume-weighted average of fine-scale gas saturation over the region corresponding to coarse gridblock m, and $\langle z_i^f \rangle_m$ is the analogous average for overall compositions of component i. The error for overall composition is normalized by the difference between the injection and initial phase compositions.
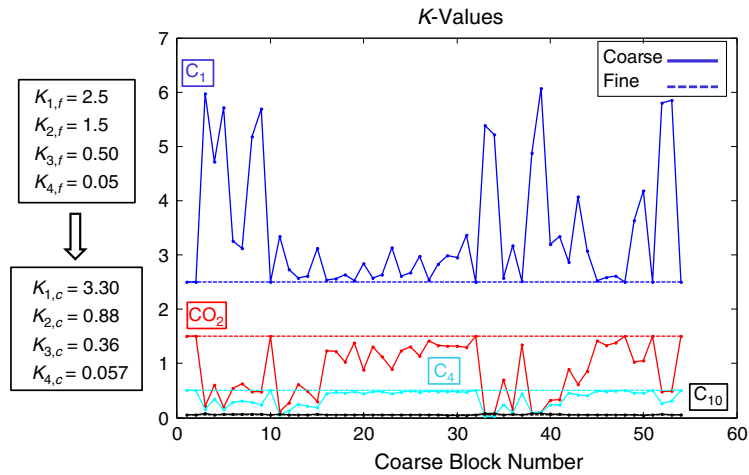

Fig. 7—Set of *K*-values for fine- and coarse-scale (22×6) simulations, Case 1.

	C$_1$	CO$_2$	NC$_4$	C$_{10}$
Fine scale (220×60)	2.5	1.5	0.50	0.05
Coarse scale (55×15)	2.9	1.15	0.42	0.053
Coarse scale (22×6)	3.3	0.88	0.36	0.057

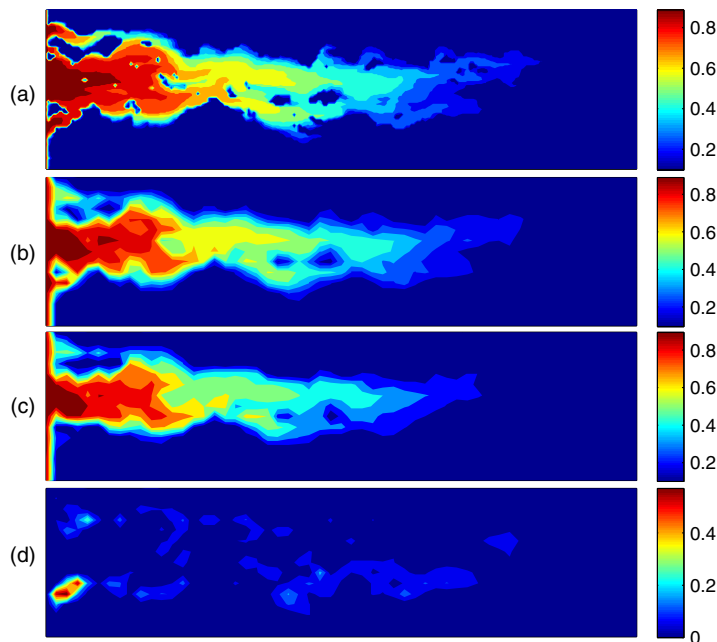Table 3—*K*-value sets for fine scale vs. coarse scale, Case 1.

Fig. 8—C$_1$ overall composition distributions for (a) fine scale, (b) averaged fine, (c) modified *K*-values coarse scale (16X upscaling), and (d) error map at 230 days, Case 1.

We also present another type of error that is calculated at the fine-scale resolution. The real difference between the fine-scale simulation and the upscaled simulation is the summation over the fine gridblocks, and for each fine gridblock takes the difference between the fine-grid value and the value in the coarse gridblock that encompasses the fine grid cell. This type of error is denoted as $E_{z_i}^f$ and is computed using similar equations as Eqs. 24 and 25, with the only distinction being summing differences over fine-scale gridblocks instead of coarse-scale gridblocks. The modified K-values approach provides results that are in a close agreement with the averaged fine-scale solutions. A summary of error analysis for both types of errors at two different upscaling ratios is provided in **Table 4.** For all the components, both types of error are larger in the case of 100X upscaling than 16X upscaling. Note that for both upscaling ratios, errors computed at fine-scale level ($E_{z_i}^f$) are higher than errors computed at coarse-scale level ($E_{z_i}^c$), which is expected because of the larger discrepancies of solutions at fine-scale resolution. **Table 5** summarizes the central-processing-unit (CPU) times for fine-scale simulation vs. SPU and K-values-based upscaling at two different upscaling ratios. As demonstrated, the additional computational cost for K-values-based upscaling vs. SPU is reasonable, considering a significant improvement in the accuracy of results.

Error (%)	C_1	CO_2	C_4	C_{10}
$E_{z_i}^c$ (upscaling ratio: 16)	4.27	6.03	4.63	4.48
$E_{z_i}^f$ (upscaling ratio: 16)	10.95	13.76	11.58	10.63
$E_{z_i}^c$ (upscaling ratio: 100)	6.2	8.31	6.65	6.55
$E_{z_i}^f$ (upscaling ratio: 100)	14.3	17.46	15.12	13.31

Table 4—Error analysis at coarse-scale resolution ($E_{z_i}^c$) and at fine-scale resolution ($E_{z_i}^f$) for components' overall composition distributions at 400 days, K-values-based upscaling, Case 1.

|	Fine Scale	SPU (16X)	K-Values (16X)	SPU (100X)	K-Values (100X)
CPU time (seconds)	591.63	20.42	47.49	3.18	5.66
Normalized CPU time	1	0.04	0.08	0.005	0.01

Table 5—Comparison of CPU times for fine-scale simulation vs. SPU and K-values-based upscaling at two different upscaling ratios, Case 1.

To test the robustness of the presented upscaling approach and evaluate the dependencies of upscaled flow and upscaled thermodynamics functions on initial boundary conditions, we switched the injection and production boundary conditions; i.e., the four-component gas—C_1 (97%), CO_2 (1%), C_4 (1%), and C_{10} (1%)—is injected through the right boundary at 100 bar and production is through the left boundary at 70 bar. Coarse-scale simulations are performed without adjusting upscaled flow and thermodynamics functions for the new set of boundary conditions. **Fig. 9** demonstrates the C_1 overall composition distributions for fine scale, averaged fine, modified K-values coarse scale, and error map at 230 days ($E_{C_1}^c = 8.26\%$). Our upscaling approach captures the fine-scale solutions even without modifying the upscaled functions in the case of reversed boundary conditions. The upscaled flow and thermodynamics functions are precomputed and stored in tables for each upstream coarse gridblock with fine-scale simulations, with relatively small timesteps and long-enough simulation time to make sure gas breakthrough has occurred and all coarse gridblocks have experienced a full saturation and phase-status change. These refined upscaled tables store a significant amount of information for direction-dependent effective-flow functions and may be used even once the boundary conditions are (moderately) changed.

Case 2: Channelized Model With Eight-Component Compositional System. Here, we apply the K-values-based compositional upscaling to a more-complex model characterized by channelized permeability fields. The permeability field is generated using SGeMS (Remy et al. 2009) and is adapted from Li (2014). The permeability distributions (log k) for fine- and coarse-scale models are shown in **Fig. 10.** The fine-scale model contains 55×55 cells, with each cell of dimensions $\Delta x = \Delta y = 15$ m and $\Delta z = 3$ m. The coarse model is generated by uniformly coarsening the fine model, containing 11×11 gridblocks. The permeability field is considered isotropic on the fine scale (i.e., $k_x = k_y$) and is scaled up using the local permeability-upscaling technique (Fig. 10b).

We consider a constant K-values displacement of initial oil, which is a mixture of eight components, and a two-component gas is injected through the left boundary at 100 bar. The compositions of initial oil and injected gas are shown in **Table 6.** This fluid system is adapted from Zaydullin (2011). Oil is produced through the right boundary at 90 bar, which is the same as initial reservoir pressure. The displacement is isothermal at 373 K and the simulation is run for 800 days. Porosity is specified as $\phi = 0.20$ (constant) for all the gridblocks. We address the details of computing K-values at fine and coarse scales (presented in Table 6) in the following subsection.

*Spatial and Temporal Variation of Upscaled **K**-Values.* In this subsection, we investigate the spatial and temporal variations of K-values for both fine- and coarse-scale simulations. **Fig. 11** shows the spatial variation of K-values for an EOS-based fine-scale model at a given timestep. **Table 7** summarizes the temporal variation of fine-scale K-values for eight different time levels. We take into account both spatial and temporal variations of EOS-based K-values to obtain the most-phase-behavior-representative K-values for the fine-scale simulation. The final averaged K-values are listed in Table 7. We also conduct both EOS-based and K-values-based fine-scale simulations to assess the errors obtained from using constant K-values. **Fig. 12** shows the C_1 overall composition distributions at 400 days from the full EOS phase-behavior model (on left) and the error map of C_1 overall composition caused by using constant K-values relative to the full EOS model (on right). Given that both spatial and temporal variations are accounted for to obtain K-values, the K-values-based fine-scale simulation results are in close agreement with EOS-based fine-scale simulation with a very small error.
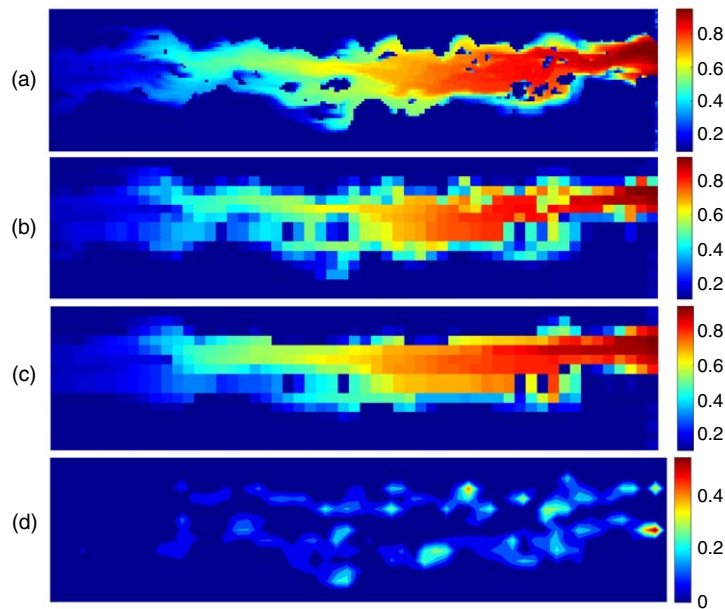
Fig. 9—Reversed boundary conditions; C_1 overall composition distributions for (a) fine scale, (b) averaged fine, (c) modified K-values coarse scale (16X upscaling), and (d) error map at 230 days, Case 1.

Fine (55×55) Coarse (11×11)

(a) (b)
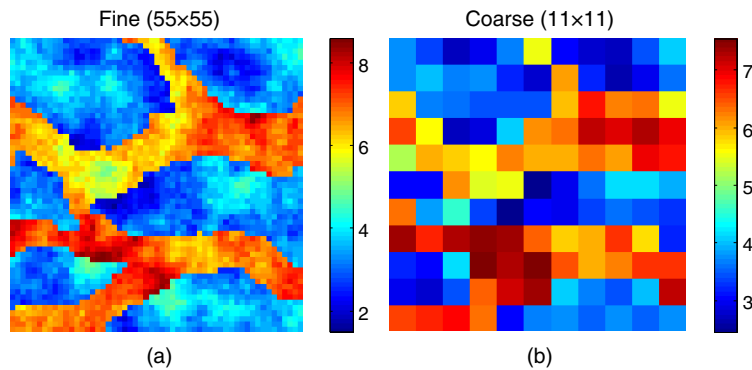
Fig. 10—Permeability fields (log k) for (a) fine scale (55×55) and (b) coarse scale (11×11), Case 2.

	C_1	CO_2	C_2	C_3	C_4	C_6	C_8	C_{15}
Initial oil	0.10	0.01	0.01	0.01	0.10	0.10	0.20	0.47
Injected gas	0.20	0.80	0	0	0	0	0	0
K_i^f	3.10	1.94	1.28	0.72	0.40	0.13	0.05	0.002
K_i^c	2.70	2.36	0.73	0.45	0.27	0.10	0.04	0.002

Table 6—Compositions of initial oil and injected gas and K-values, Case 2.
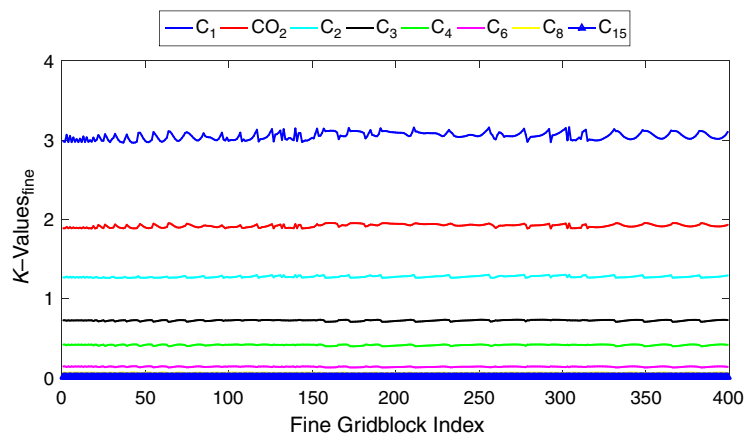
Fig. 11—Spatial variation of K-values for EOS-based fine-scale model, Case 2.

	C_1	CO_2	C_2	C_3	C_4	C_6	C_8	C_{15}
Time = 100 days	3.0519	1.9164	1.2712	0.7181	0.4077	0.1329	0.0553	0.0027
Time = 200 days	3.0749	1.9275	1.2757	0.7187	0.4070	0.1319	0.0547	0.0026
Time = 300 days	3.0960	1.9379	1.2811	0.7203	0.4071	0.1315	0.0544	0.0026
Time = 400 days	3.1068	1.9439	1.2835	0.7209	0.4070	0.1312	0.0542	0.0026
Time = 500 days	3.1194	1.9498	1.2858	0.7211	0.4065	0.1307	0.0539	0.0025
Time = 600 days	3.1298	1.9545	1.2879	0.7215	0.4063	0.1303	0.0536	0.0025
Time = 700 days	3.1326	1.9563	1.2880	0.7213	0.4060	0.1301	0.0535	0.0025
Time = 800 days	3.1365	1.9584	1.2800	0.7213	0.4057	0.1299	0.0534	0.0025
K_i^f (average)	3.1060	1.9431	1.2816	0.7204	0.4067	0.1311	0.0541	0.0026

Table 7—Temporal variation of fine-scale K-values (conversion from full EOS model to constant K-values), Case 2.

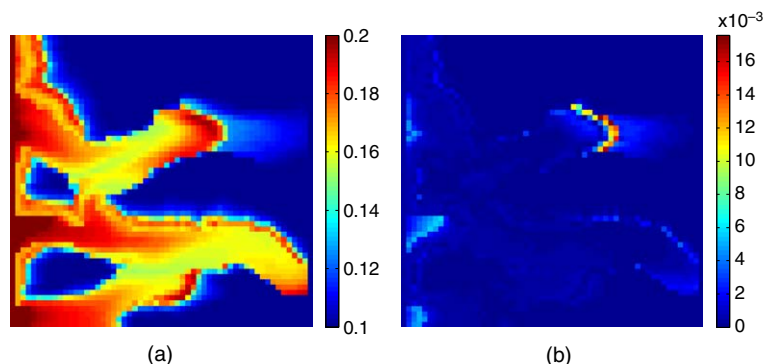(a)   (b)

Fig. 12—(a) C_1 overall composition distributions at 400 days from full EOS phase-behavior model; (b) error in C_1 overall composition caused by using constant K-values relative to the full EOS model, Case 2.

The same analysis is performed for spatial and temporal variations of coarse-scale K-values. **Fig. 13** shows the spatial variation of K-values for a nonequilibrium EOS-based coarse-scale model at a given timestep. Note that the coarse-scale K-values are shown only for two-phase coarse gridblocks, and the rest of the coarse gridblocks are in single-phase initial oil status. **Table 8** summarizes the temporal variation of coarse-scale K-values for eight different time levels. Both spatial and temporal variations of nonequilibrium EOS-based K-values are taken into account to obtain the most-phase-behavior-representative K-values for the coarse-scale simulation. The final averaged K-values for coarse-scale simulation are listed in Table 8. Note that in addition to the upscaled K-values, the single-phase and two-phase upscaled flow functions are also required for the coarse-scale simulation.
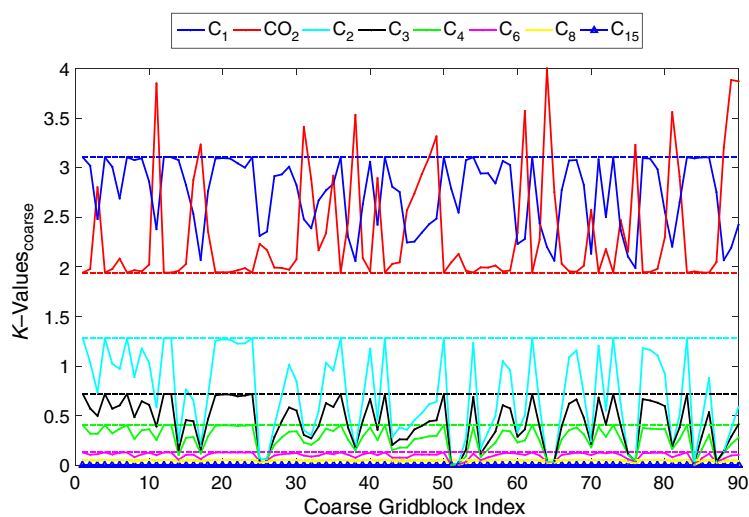

Fig. 13—Spatial variation of K-values for fine scale (55×55) in dashed lines and coarse scale (11×11) in solid lines, Case 2.

Fig. 14 displays CO_2-concentration maps at 400 days for the fine scale, averaged fine, SPU, and modified K-values upscaling. We clearly see substantial gas channeling in the fine-scale model. Compared with the averaged fine-scale result, the SPU solution (Fig. 14c) displays a significantly delayed gas front and higher gas saturations near the inlet edge, which eventually results in overestimation of gas-breakthrough time. The modified K-values upscaling approach, by contrast, provides a significant improvement in the results, and

generates highly accurate solutions over the entire simulation time frame. **Table 9 and Fig. 15** summarize the error values for the overall compositions of all the components. As demonstrated, the modified K-values approach provides results in a close agreement with the nonequilibrium approach by using a much-lower computational cost. Note that errors computed at fine-scale level ($E_{z_i}^f$) are higher than errors computed at coarse-scale level ($E_{z_i}^c$), which is expected because of the larger discrepancies of solutions at fine-scale resolution. The nonequilibrium results are obtained using the two-parameter Peng and Robinson (1976) EOS. **Table 10** summarizes the CPU times for fine-scale simulation vs. SPU, nonequilibrium EOS-based upscaling, and K-values-based upscaling. As demonstrated, the additional computational cost for K-values-based upscaling vs. SPU is reasonable, considering significant improvement in the accuracy of the results.

	C_1	CO_2	C_2	C_3	C_4	C_6	C_8	C_{15}
Time = 100 days	2.7598	2.3064	0.8890	0.5245	0.3103	0.1095	0.0477	0.0027
Time = 200 days	2.6298	2.4535	0.7269	0.4456	0.2733	0.1023	0.0461	0.0026
Time = 300 days	2.6178	2.4092	0.6983	0.4325	0.2675	0.1017	0.0463	0.0026
Time = 400 days	2.6574	2.3602	0.7131	0.4411	0.2723	0.1022	0.0463	0.0026
Time = 500 days	2.6932	2.3461	0.7135	0.4404	0.2717	0.1021	0.0460	0.0026
Time = 600 days	2.7344	2.3017	0.7149	0.4402	0.2703	0.1015	0.0457	0.0026
Time = 700 days	2.7395	2.3438	0.7130	0.4404	0.2706	0.1014	0.0456	0.0026
Time = 800 days	2.7471	2.3439	0.7049	0.4364	0.2686	0.1007	0.0453	0.0026
K_i^c (average)	2.6974	2.3581	0.7342	0.4501	0.2756	0.1027	0.0461	0.0026

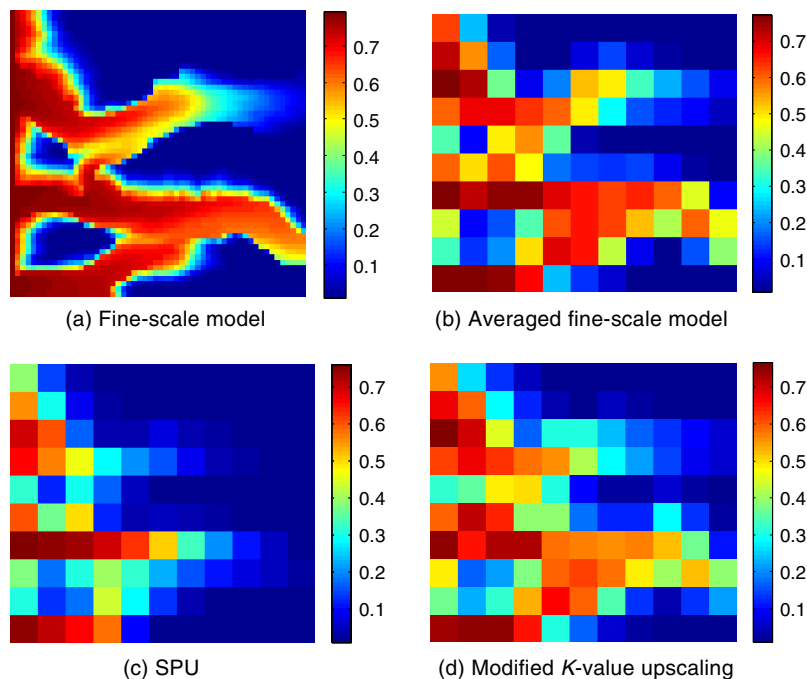Table 8—Temporal variation of coarse-scale K-values (conversion from full EOS model to constant K-values), Case 2.

(a) Fine-scale model

(b) Averaged fine-scale model

(c) SPU

(d) Modified K-value upscaling

Fig. 14—CO_2 overall composition distributions at 400 days, Case 2.

Error (%)	C_1	CO_2	C_2	C_3	C_4	C_6	C_8	C_{15}
$E_{z_i}^c$, modified K-values	11.7	9.1	11.7	10.7	9.9	9.1	8.8	8.8
$E_{z_i}^c$, nonequilibrium	11.2	8.6	9.5	9.1	8.9	8.6	8.6	8.7
$E_{z_i}^f$, modified K-values	17.1	15.8	16.2	15.8	14.8	13.7	13.4	13.3
$E_{z_i}^f$, nonequilibrium	16.4	15.1	15.3	14.9	13.9	13.2	12.9	12.8

Table 9—Error analysis at coarse-scale resolution ($E_{z_i}^c$) and at fine-scale resolution ($E_{z_i}^f$) for components' overall composition distributions at 400 days, Case 2.
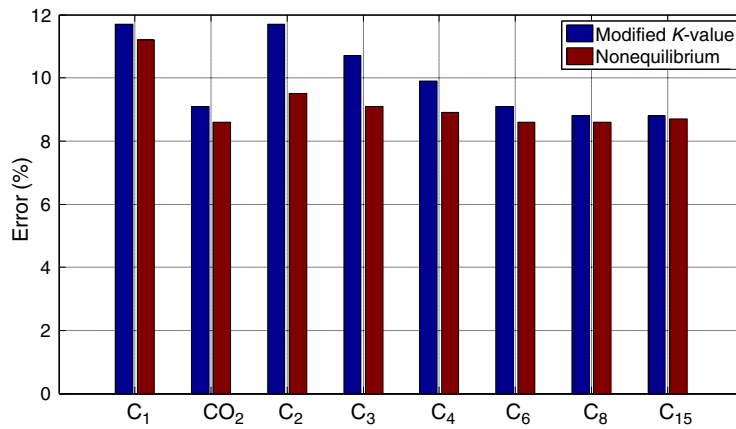
Fig. 15—Error analysis (at coarse-scale resolution, $E_{z_i}^c$) for components' overall composition distributions at 400 days, Case 2.

	Fine Scale	SPU	NE	*K*-Values
CPU time (seconds)	169.15	9.03	50.59	21.67
Normalized CPU time	1	0.05	0.30	0.12

Table 10—Comparison of CPU times for fine-scale simulation vs. SPU, nonequilibrium upscaling (NE), and *K*-values-based upscaling, Case 2.

Conclusions

We presented a general fine-scale compositional simulation framework. EOS-based phase equilibrium calculations are responsible for a significant fraction of computational time in compositional reservoir simulations. We simplified the EOS computations by assuming that components partition across phases with a fixed ratio (equilibrium constant or *K*-value). The *K*-values-based compositional simulation framework reduces the computational cost of simulation. We introduced a *K*-values-based coarse-scale operator for compositional simulation. Upscaled nonequilibrium thermodynamics functions are used to transform the equilibrium phase space from the fine scale to a modified region of similar shape, but with tilted tie-lines on the coarse scale. Using the orientation of tie-lines in the new nonequilibrium phase space and the sign of upscaled thermodynamics functions, we developed a framework to obtain a modified set of *K*-values. We showed that use of standard coarse models (with only upscaled transmissibilities and flow functions) is often not sufficient to capture the fine-scale compositional solutions and lead to inaccurate solutions. The modified *K*-values along with upscaled single-phase- and two-phase-flow parameters are then used for coarse-scale compositional simulation of various challenging gas-injection problems with large numbers of components and highly heterogeneous permeability fields. We showed that the modified *K*-values improve the accuracy of coarse-scale solutions in reproducing averaged fine-scale solutions, such as components' overall compositions and phase-saturation distributions. Future work directions include developing local/global upscaling frameworks to compute upscaled functions more efficiently, and extension of the current upscaling formulation to three-phase systems.

Nomenclature

f_{ij} = fugacity of component i in phase j
$\mathbf{k}$ = absolute permeability
k_r = relative permeability
N_b = number of gridblocks
N_c = number of components
N_p = number of phases
p = pressure
P_c = critical pressure
q = source/sink
Q = volumetric source/sink
S = phase saturation
t = time
T = geometric transmissibility
T_c = critical temperature
u = Darcy velocity
ν_j = molar fraction of phase j
V = bulk volume
x_{ij} = mole fraction of component i in phase j
z = overall composition
$\Delta x, \Delta y, \Delta z$ = gridblock dimensions
λ_j = mobility of phase j
μ_j = viscosity of phase j
ρ_j = molar density of phase j
ϕ = porosity

$\hat{\phi}_{ij}$ = partial fugacity coefficient of component i in phase j
ω = acentric factor
$\triangledown$ = divergence or gradient

Superscripts
$*$ = upscaled property or function
c = coarse-scale variable
f = fine-scale variable
inj = injector property
l = index of fine gridblock or interface
prod = producer property

Subscripts
g = gas phase
i = component
j = phase
l = index of fine gridblock or interface
m = index of coarse gridblock
o = oil phase
t = total quantity

Acknowledgment

References
Aziz, K. and Wong, T. W. 1988. Considerations in the Development of Multipurpose Reservoir Simulation Models. *Proc.,* 1st and 2nd International Forum on Reservoir Simulation, Alpbach, Austria, 12–16 September, 77–208.

Ballin, P. R., Clifford, P. J., and Christie, M. A. 2002. Cupiagua: Modeling of a Complex Fractured Reservoir Using Compositional Upscaling. *SPE Res Eval & Eng* **5** (6): 488–498. SPE-81409-PA. https://doi.org/10.2118/81409-PA.

Barker, J. W. and Dupouy, P. 1999. An Analysis of Dynamic Pseudo-Relative Permeability Methods for Oil-Water Flows. *Petrol. Geosci.* **5** (4): 385–394. https://doi.org/10.1144/petgeo.5.4.385.

Barker, J. W. and Fayers, F. J. 1994. Transport Coefficients for Compositional Simulation With Coarse Grids in Heterogeneous Media. *SPE Advances Technology Series* **2** (2): 103–112. SPE-22591-PA. https://doi.org/10.2118/22591-PA.

Barker, J. W. and Thibeau, S. 1997. A Critical Review of the Use of Pseudorelative Permeabilities for Upscaling. *SPE Res Eval & Eng* **12** (2): 138–143. SPE-35491-PA. https://doi.org/10.2118/35491-PA.

Bolling, J. D. 1987. Development and Application of a Limited-Compositional, Miscible Flood Reservoir Simulator. Presented at the SPE Symposium on Reservoir Simulation, San Antonio, Texas, 1–4 February. SPE-15998-MS. https://doi.org/10.2118/15998-MS.

Cao, H. 2002. *Development of Techniques for General Purpose Simulators*. PhD dissertation, Stanford University, Stanford, California.

Chen, Y. and Durlofsky, L. J. 2006. Efficient Incorporation of Global Effects in Upscaled Models of Two-Phase Flow and Transport in Heterogeneous Formations. *Multiscale Model. Simul.* **5** (2): 445–475. https://doi.org/10.1137/060650404.

Chen, Y., Durlofsky, L. J., Gerritsen, M. et al. 2003. A Coupled Local-Global Upscaling Approach for Simulating Flow in Highly Heterogeneous Formations. *Adv. Water Resour.* **26** (10): 1041–1060. https://doi.org/10.1016/S0309-1708(03)00101-5.

Christie, M. A. 1996. Upscaling for Reservoir Simulation. *J Pet Technol* **48** (11): 1004–1010. SPE-37324-JPT. https://doi.org/10.2118/37324-JPT.

Christie, M. A. and Blunt, M. J. 2001. Tenth SPE Comparative Solution Project: A Comparison of Upscaling Techniques. *SPE Res Eval & Eng* **4** (4): 308–317. SPE-72469-PA. https://doi.org/10.2118/72469-PA.

Christie, M. A. and Clifford, P. J. 1998. Fast Procedure for Upscaling Compositional Simulation. *SPE J.* **3** (3): 272–278. SPE-50992-PA. https://doi.org/10.2118/50992-PA.

Coats, K. H. 1980. An Equation of State Compositional Model. *SPE J.* **20** (5): 363–376. SPE-8284-PA. https://doi.org/10.2118/8284-PA.

Coats, K. H., Thomas, L. K., and Pierson, R. G. 2004. Simulation of Miscible Flow Including Bypassed Oil and Dispersion Control. Presented at the SPE Annual Technical Conference and Exhibition, Houston, 26–29 September. SPE-90898-MS. https://doi.org/10.2118/90898-MS.

Darman, N. H., Pickup, G. E., and Sorbie, K. S. 2002. A Comparison of Two-Phase Dynamic Upscaling Methods Based on Fluid Potentials. *Computat. Geosci.* **6** (1): 5–27. https://doi.org/10.1023/A:1016572911992.

Durlofsky, L. J. 1991. Numerical Calculation of Equivalent Grid Block Permeability Tensors for Heterogeneous Porous Media. *Water Resour. Res.* **27** (5): 699–708. https://doi.org/10.1029/91WR00107.

Durlofsky, L. J. and Chen, Y. 2012. Uncertainty Quantification for Subsurface Flow Problems Using Coarse-Scale Models. In *Numerical Analysis of Multiscale Problems: Lecture Notes in Computational Science and Engineering*, Vol. 83, 163–202. Berlin: Springer.

Evazi, M. and Jessen, K. 2014. Dual-Porosity Coarse-Scale Modeling and Simulation of Highly Heterogeneous Geomodels. *Transport Porous Med.* **105** (1): 211–233. https://doi.org/10.1007/s11242-014-0367-7.

Farmer, C. L. 2002. Upscaling: A Review. *Int. J. Numer. Meth. Fl.* **40** (1–2): 63–78. https://doi.org/10.1002/fld.267.

Fayers, F. J., Barker, J. W., and Newley, T. M. J. 1989. Effects of Heterogeneities on Phase Behaviour in Enhanced Oil Recovery. Oral presentation given at ECMOR I–1st European Conference on the Mathematics of Oil Recovery, Cambridge, UK, 1 July.

Hui, M. H. 2005. *Upscaling of Multiphase Flow Parameters for Modeling Near-Well and Miscible Displacements*. PhD dissertation, Stanford University, Stanford, California.

Indrupskiy, I. M., Lobanova, O. A., and Zubov, V. R. 2016. Non-Equilibrium Phase Behavior of Hydrocarbons in Compositional Simulations and Upscaling. Oral presentation given at ECMOR XV–15th European Conference on the Mathematics of Oil Recovery, Amsterdam, 29 August–1 September.

Iranshahr, A., Chen, Y., and Voskov, D. V. 2014. A Coarse-Scale Compositional Model. *Computat. Geosci.* **18** (5): 797–815. https://doi.org/10.1007/s10596-014-9427-x.

Iranshahr, A., Voskov, D. V., and Tchelepi, H. A. 2013a. A Negative-Flash Tie-Simplex Approach for Multiphase Reservoir Simulation. *SPE J.* **18** (6): 1140–1149. SPE-141896-PA. https://doi.org/10.2118/141896-PA.

Iranshahr, A., Voskov, D. V., and Tchelepi, H. A. 2013b. Tie-Simplex Based Compositional Space Parameterization: Continuity and Generalization to Multiphase Systems. *AIChE J.* **59** (5): 1684–1701. https://doi.org/10.1002/aic.13919.

Juanes, R. 2008. A Robust Negative Flash Based on a Parameterization of the Tie-Line Field. *Fluid Phase Equilibr.* **267** (1): 6–17. https://doi.org/10.1016/j.fluid.2008.02.009.

Kyte, J. R. and Berry, D. W. 1975. New Pseudo Functions to Control Numerical Dispersion. *SPE J.* **15** (4): 269–276. SPE-5105-PA. https://doi.org/10.2118/5105-PA.

Li, H. 2014. *Compositional Upscaling for Individual Models and Ensembles of Realizations*. PhD dissertation, Stanford University, Stanford, California.

Li, H. and Durlofsky, L. J. 2016. Upscaling for Compositional Reservoir Simulation. *SPE J.* **21** (3): 873–887. https://doi.org/10.2118/173212-PA.

Michelsen, M. L. 1982a. The Isothermal Flash Problem. Part I. Stability. *Fluid Phase Equilibr.* **9** (1): 1–19. https://doi.org/10.1016/0378-3812(82)85001-2.

Michelsen, M. L. 1982b. The Isothermal Flash Problem. Part II. Phase-Split Calculation. *Fluid Phase Equilibr.* **9** (1): 21–40. https://doi.org/10.1016/0378-3812(82)85002-4.

Ogunlana, D. O. and Mohanty, K. K. 2005. Compositional Upscaling in Fractured Reservoirs During Gas Recycling. *J. Pet. Sci. Eng.* **46** (1–2): 1–21. https://doi.org/10.1016/j.petrol.2004.11.004.

Orr, F. M. 2007. *Theory of Gas Injection Processes*. Holte, Denmark: Tie-Line Publications.

Pan, H. and Tchelepi, H. A. 2011. Compositional Flow Simulation Using Reduced-Variables and Stability-Analysis Bypassing. Presented at the SPE Reservoir Simulation Symposium, The Woodlands, Texas, 21–23 February. SPE-142189-MS. https://doi.org/10.2118/142189-MS.

Peng, D. Y. and Robinson, D. B. 1976. A New Two-Constant Equation of State. *Int. Eng. Chem. Fundamen.* **15** (1): 59–64. https://doi.org/10.1021/i160057a011.

Peng, X., Du, Z., Liang, B., and Qi, Z. 2009. Darcy-Stokes Streamline Simulation for the Tahe-Fractured Reservoir With Cavities. *SPE J.* **14** (3): 543–552. SPE-107314-PA. https://doi.org/10.2118/107314-PA.

Rannou, G., Voskov, D. V., and Tchelepi, H. A. 2013. Tie-Line-Based *K*-Value Method for Compositional Simulation. *SPE J.* **18** (06): 1112–1122. SPE-167257-PA. https://doi.org/10.2118/167257-PA.

Rasmussen, C. P., Krejbjerg, K., Michelsen, M. L. et al. 2003. Increasing Computational Speed of Flash Calculations With Applications for Compositional, Transient Simulations. Presented at the SPE Annual Technical Conference and Exhibition, Denver, 5–8 October. SPE-84181-MS. https://doi.org/10.2118/84181-MS.

Remy, N., Boucher, A., and Wu, J. 2009. *Applied Geostatistics With SGeMS: A User's Guide*. Cambridge, UK: Cambridge University Press.

Salehi, A. 2016. *Upscaling of Compositional Flow Simulation Based on a Non-Equilibrium Formulation*. PhD dissertation, Stanford University, Stanford, California.

Salehi, A., Voskov, D. V., and Tchelepi, H. A. 2012. Upscaling of Compositional Flow Simulation Based on a Non-Equilibrium Formulation. Oral presentation given at the American Geophysical Union Fall Meeting, San Francisco, 3–7 December.

Salehi, A., Voskov, D. V., and Tchelepi, H. A. 2013. Thermodynamically Consistent Transport Coefficients for Upscaling of Compositional Processes. Presented at the SPE Reservoir Simulation Symposium, The Woodlands, Texas, 18–20 February, SPE-163576-MS. https://doi.org/10.2118/163576-MS.

Shirangi, M. G. and Durlofsky, L. J. 2015. Closed-Loop Field Development Under Uncertainty by Use of Optimization With Sample Validation. *SPE J.* **20** (5): 908–922. SPE-173219-PA. https://doi.org/10.2118/173219-PA.

Stone, H. L. 1991. Rigorous Black Oil Pseudo Functions. Presented at the SPE Symposium on Reservoir Simulation, Anaheim, California, 17–20 February. SPE-21207-MS. https://doi.org/10.2118/21207-MS.

Volkov, O. and Voskov, D. V. 2016. Effect of Time Stepping Strategy on Adjoint-Based Production Optimization. *Computat. Geosci.* **20** (3): 707–722. https://doi.org/10.1007/s10596-015-9528-1.

Voskov, D. 2012. An Extended Natural Variable Formulation for Compositional Simulation Based on Tie-Line Parameterization. *Transport Porous Med.* **92** (3): 541–557. https://doi.org/10.1007/s11242-011-9919-2.

Voskov, D. V. and Tchelepi, H. A. 2009a. Compositional Space Parameterization: Theory and Application for Immiscible Displacements. *SPE J.* **14** (3): 431–440. SPE-106029-PA. https://doi.org/10.2118/106029-PA.

Voskov, D. V. and Tchelepi, H. A. 2009b. Compositional Space Parameterization: Multicontact Miscible Displacements and Extension to Multiple Phases. *SPE J.* **14** (3): 441–449. SPE-113492-PA. https://doi.org/10.2118/113492-PA.

Voskov, D. V. and Tchelepi, H. A. 2012. Comparison of Nonlinear Formulations for Two-Phase Multi-Component EOS Based Simulation. *J. Pet. Sci. Eng.* **82–83** (February–March): 101–111. https://doi.org/10.1016/j.petrol.2011.10.012.

Wallstrom, T. C., Christie, M. A., Durlofsky, L. J. et al. 2002. Effective Flux Boundary Conditions for Upscaling Porous Media Equations. *Transport Porous Med.* **46** (2–3): 139–153. https://doi.org/10.1023/A:1015075210265.

Wu, X. H., Parashkevov, R., Stone, M. et al. 2008. Global Scale-Up on Reservoir Models With Piecewise Constant Permeability Field. *J. Algorithm. Computat. Technol.* **2** (2): 223–247. https://doi.org/10.1260/174830108784646643.

Zaydullin, R. 2011. *Direct Discretization of the Tie-Line Space for Compositional Flow Simulation*. Master's thesis, Stanford University, Stanford, California.

Zhang, B. and Okuno, R. 2015. Modeling of Capacitance Flow Behavior in EOS Compositional Simulation. *J. Pet. Sci. Eng.* **131** (July): 96–113. https://doi.org/10.1016/j.petrol.2015.04.014.

Zhang, P., Pickup, G. E., and Christie, M. A. 2008. A New Practical Method for Upscaling in Highly Heterogeneous Reservoir Models. *SPE J.* **13** (1): 68–76. SPE-103760-PA. https://doi.org/10.2118/103760-PA.

Zhou, Y. 2012. *Parallel General-Purpose Reservoir Simulation With Coupled Reservoir Models and Multi-Segment Wells*. PhD dissertation, Stanford University, Stanford, California.

Zhou, Y., Tchelepi, H. A., and Mallison, B. T. 2011. Automatic Differentiation Framework for Compositional Simulation on Unstructured Grids With Multi-Point Discretization Schemes. Presented at the SPE Reservoir Simulation Symposium, The Woodlands, Texas, 21–23 February. SPE-141592-MS. https://doi.org/10.2118/141592-MS.

Zubov, V. R., Indrupskiy, I. M., and Bogachev, K. Y. 2016. Compositional Simulator With Non-Equilibrium Phase Transitions. Presented at the SPE Russian Petroleum Technology Conference and Exhibition, Moscow, 24–26 October. SPE-182001-MS. https://doi.org/10.2118/182001-MS.

Amir Salehi is technical team lead of reservoir modeling and forecasting at Quantum Reservoir Impact. His research interests include upscaling and multiscale modeling methods for reservoir-simulation models with complex physics; new approaches for compositional modeling; general-purpose simulation of multiphase multicomponent flow in porous media; modeling of CO_2-sequestration processes; and data-driven reservoir modeling. Salehi holds a bachelor's degree from Petroleum University of Technology, Iran; a master's degree from National Polytechnic Institute, France; and a PhD degree from Stanford University, all in petroleum engineering.

Denis V. Voskov joined Delft University of Technology in 2015 as an associate professor with the Department of Geoscience and Engineering. He is leading a group on modeling of flow and transport in the presence of complex physical processes in deep subsurface. Voskov previously worked at Stanford University as a senior researcher. Before Stanford University, he was a chief engineer at YUKOS Company, founder and chief technology officer of Rock Flow Dynamics Company, and a leading specialist at the Institute for Problems in Mechanics at the Russian Academy of Sciences.

Hamdi A. Tchelepi is a professor at Stanford University and codirector of the Center for Computational Earth and Environmental Science. His research covers various aspects of numerical modeling of flow and transport in natural porous media. Specific interests include analysis of unstable miscible and immiscible flows in heterogeneous formations; scalable (efficient for large problems) linear and nonlinear solution algorithms of multiphase flow in highly heterogeneous systems; and stochastic-moment-equation methods for quantifying the uncertainty associated with predictions of flow performance in the presence of limited reservoir-characterization data.